Experimental Neurology 313 (2019) 37–48

Contents lists available at ScienceDirect

Experimental Neurology

journal homepage: www.elsevier.com/locate/yexnr

Research paper

Significant changes in circular RNA in the mouse cerebral cortex around an injury site after traumatic brain injury

Zhihao Chen[a], Hong Wang[a], Jianjun Zhong[b,*], Junqing Yang[a], Rami Darwazeh[b], Xiaocui Tian[a], Zhijian Huang[b], Li Jiang[b], Chongjie Cheng[b], Yue Wu[b], Zongduo Guo[b], Xiaochuan Sun[b,*]

[a] Department of Pharmacology, Chongqing Medical University, The Key Labratory of Biochemistry and Molecular Pharmacology, Chongqing 400016, China
[b] Department of Neurosurgery, The First Affiliated Hospital of Chongqing Medical University, Chongqing 400016, China

ARTICLE INFO

Keywords:
TBI
Circular RNA
miRNA
CXCR2
RNA-seq

ABSTRACT

Background and objective: Circular RNA (circRNA) is an important type of non-coding RNA that has not been widely researched in traumatic brain injury (TBI). The present study aimd to detect the altered circRNA expression around an injury site in the mouse cerebral cortex after TBI and explore its potential functions.

Method: C57BL/6 mice were used to construct a controlled cortical impact (CCI) model to simulate TBI. At 24 h post-TBI, the cortex around the injury site was collected, and the total RNA was extracted to perform RNA sequencing (RNA-seq). The differentially expressed circRNAs were determined according to the following criteria: $|\log_2^{(\text{fold change})}| > 1, P < .05$ and FDR < 0.05. Among them, circRNA chr8_87,859,283–87,904,548 was preliminarily explored to determine its function.

Results: A total of 8036 altered circRNAs were discovered, and among them, 16 were significantly changed (5 up-regulated and 11 down-regulated). The circRNA chr8_87,859,283–87,904,548 significantly increased by approximately 4 times in the cerebral cortex around the injury site after TBI and promoted neuro-inflammation through increasing the CXCR2 protein by sponging mmu-let-7a-5p. As a result, the increased circRNA chr8_87,859,283–87,904,548 blocked the restoration of neurological function after TBI.

Conclusion: Many circRNAs are significantly up-regulated or down-regulated in the traumatic cerebral penumbra cortex after TBI. Among them, the circRNA chr8_87,859,283–87,904,548 potentially plays a pro-inflammatory role, which may have a deleterious effect on neurological restoration after TBI.

1. Introduction

Traumatic brain injury (TBI) can be divided into two phases: initial injury and secondary injury. The initial injury can be worsened by the secondary injury, resulting in an enhanced inflammatory response and increased cell death, leading to deficits in neurological function (O'Connor et al., 2011; Villapol et al., 2012; Zhong et al., 2017a). The initial injury cannot be changed, but secondary injury can be mitigated by effective therapy. Although many efforts have been made in the past decades, TBI remains a severe disease with high mortality and morbidity, and the available therapeutic strategies are limited(Liu et al., 2014; Werner and Engelhard, 2007), which results in severe economic burden to societies and families (Loane and Faden, 2010). The complex biological mechanisms underlying brain damage still need to be elucidated (Liu et al., 2014).

In mammalian cells, ~90% of eukaryotic genomes are transcribed (Wilhelm et al., 2008), and only 1 to 2% of the genome can transcribed into mRNA to encode proteins (Birney et al., 2007), suggesting that the majority of transcripts are non-coding RNA (ncRNA) and do not encode protein. The ncRNA consists of two major classes: 1) the linear ncRNA, which is presented as a linearizing strand including microRNA (miRNA) and long noncoding RNA (lncRNA), and 2) circular RNA (circRNA), which is a novel class of non-protein coding transcripts with a loop structure. CircRNA molecules are transcribed and spliced from the exons of coding or non-coding genes and express across the eukaryotic tree of life (Salzman, 2016; Ho et al., 2016). It has been proven that circRNA is substantially enriched in the mouse brain and may be involved in synaptic proteins (You et al., 2015). Moreover, circRNAs are involved in several diseases, such as glioma (Song et al., 2016), Alzheimer's disease, cerebral ischemic stroke (Han et al., 2018; Zhang et al., 2018), and temporal lobe epilepsy (Li et al., 2018). In addition, circRNA is related to brain (Veno et al., 2015) and fetal development

* Corresponding authors.
E-mail addresses: zjjcom682161@126.com (J. Zhong), sunxch1445@qq.com (X. Sun).

https://doi.org/10.1016/j.expneurol.2018.12.003
Received 27 July 2018; Received in revised form 30 October 2018; Accepted 4 December 2018
Available online 05 December 2018
0014-4886/

(Szabo et al., 2015), oxygen-glucose deprivation/reoxygenation (OGD/R)-induced neuronal injury (Lin et al., 2016), periventricular white matter damage (Zhu et al., 2018) and blood-brain barrier integrity (Bai et al., 2018), suggesting its potential regulating functions. We hypothesized that circRNA may be involved in the complex biological mechanisms underlying secondary brain damage after TBI.

No available study has explored circRNA changes after TBI in mice. Therefore, to understand the circRNA landscape around the injury site in the mouse cerebral cortex after TBI, we used a high-throughput RNA sequencing technique to measure circRNA changes in the peri-contusion areas after TBI. A total of 16 circRNAs changed in the traumatic cerebral cortex after TBI. The enriched pathway, biological process, cellular components and molecular function of the altered circRNAs were explored through bioinformatics. The potential regulating network between the differentially expressed circRNAs, mRNAs and miRNAs was also constructed by bioinformatic calculation. The circRNA chr8_87,859,283–87,904,548 significantly increased approximately 4 times after TBI and was chosen for subsequent exploration of its potential roles. Our results suggest that circRNA chr8_87,859,283–87,904,548 may play a pro-inflammatory role, which may cause a deleterious effect on neurological restoration after TBI.

2. Methods and materials

2.1. Animals

Adult male C57BL/6 mice (n = 228), aged 12 weeks and weighing 20 to 22 g, were obtained from the Experimental Animal Center of Chongqing Medical University (Chongqing, China) and were divided into 5 groups: 1) a sham group (which received only a craniotomy, not TBI impact nor any treatment, n = 15); 2) TBI group (which received only TBI, n = 45); 3) Ad-GFP + TBI group (which received TBI and Ad-GFP virus, n = 45); 4) Ad-cirRNA-Chr-8 + TBI group (which received TBI and Ad-cirRNA-Chr-8 virus, n = 45); and 5) mimic + TBI group (which received TBI and mimic, n = 45). In addition, 18 mice were used to perform the RNA sequencing assay, and another 15 mice were used to explore whether mimic could reverse the increased CXCR2. All mice were housed in cages with a 12-h light/dark cycle, with food and water *ad libitum*. For anesthesia induction, mice were administered with 3% isoflurane in 67% N_2O / 30% O_2 until they were unresponsive to the tail pinch test, and then 1.5% isoflurane for anesthesia maintenance (Zhong et al., 2017a).

2.2. Ethic statement

All procedures in the present study were approved by the Animal Care and Use Committee of Chongqing Medical University. We followed the ethical guidelines according to the ARRIVE standards. All surgeries were performed under general anesthesia and efforts were made to minimize the number of animals used and reduce suffering.

2.3. TBI model

The controlled cortical impact (CCI) model was used to simulate TBI. As described in our previous study (Rola et al., 2006), CCI was conducted according to the following parameters: velocity 5.0 m/s; depth 2.0 mm and dwelling time100 ms [21 − 23].

2.4. CircRNA identification and quantification

At 24 h post-CCI, mice (n = 18) were anesthetized and decapitated. The RNA in peri-contusion areas of the brain cortex was isolated, purified and reversely transcribed to construct a cDNA library. The purified library products were finally subjected to RNA sequencing on a HiSeq 2500 platform(Rola et al., 2006). All valid sequencing data were processed using the following steps: 1) aligned to the mouse genome (http://genome.ucsc.edu/) (Rola et al., 2006); 2) discarded the reads that were contiguously aligned to the genomes; and 3) the unmapped reads were subjected to special analysis for back-splice junction sites using three algorithms (CIRI, circRNA-finder and find-circ)(Xia et al., 2017) to identify the possible circRNAs. CircRNA candidates were reported if the head-to-tail junction was supported by at least two reads and the splicing score was greater than or equal to 10(You et al., 2015). Genes that gave rise to individual circRNAs were identified by matching the genomic location of circRNAs to the location of the genes detected by TopHat/Cufflinks using BED tools(Veno et al., 2015). The DEGseq software (v1.14.0, Tsinghua University, China) was used to identify the differentially expressed circRNA based on the following criteria: $|\log_2^{(\text{fold change})}| > 1$, $P < .05$ and FDR < 0.05(Rola et al., 2006).

2.5. Potential miRNA binding sites

To identify and quantify the miRNA binding sites on circRNA, the exonic sequences within each circRNA were concatenated using Ensembl annotation. The number of predicted binding sites (7mer-m8) for all miRNAs (deposited in miRBase version 19) was counted. The same procedure was performed on CDS and 3′-untranslational region (3'-UTR) of mRNA(You et al., 2015).

2.6. KEGG pathway and gene ontology analyses

Kyoto Encyclopedia of Genes and Genomes (KEGG) pathway (http://www.genome.jp) and Gene Ontology (GO) analyses of the circRNA-derived genes were performed to predict the potential biological roles of the circRNA. The rules of "$P < 0.05$ as well as FDR < 0.05" were used as thresholds to define the significantly enriched GO terms and pathways(Rola et al., 2006).

2.7. Network analysis

CircRNA may regulate mRNA through sequestering their common miRNAs. The reciprocally regulating network between circRNAs and mRNAs was constructed based on the intermediary miRNAs to explore the potential roles of the circRNAs.

2.8. HT22 cells and BV2 cells culture

The immortalized mouse hippocampal neuron line (HT22) (Salvi et al., 2016) was purchased from JENNIO Biological Technology (Guangzhou, China) and was cultured in Dulbecco's Modified Eagle's Medium (DMEM, Gibco, Carlsbad, USA), including 10% fetal bovine serum (FBS). A microglial cell line (BV2) (Bhat et al., 2016; Zhang et al., 2016) was purchased from China Infrastructure of Cell Line Resources (Shanghai, China) and was grown in DMEM medium, including 10% FBS. To infect cells, a virus was added and diluted to 2×10^6 pfu/mL at 2 h after seeding. Lipopolysaccharide (LPS) was dissolved in serum-free culture medium for a final concentration of approximately 200 ng/ml. At 24 h after LPS treatment, the culture medium was collected, and the total protein was harvested to measure the cytokines.

2.9. RT-qPCR

RT-PCR was performed in the following reaction system: 3.6 μL RNase-free H2O, 0.2 μL forward primer (5 μM), 0.2 μL reverse primer (5 μM), 1 μL cDNA template, 5 μL SYBR green supermix (1,725,150, and iTaq™ Universal SYBR® Green, BioRad, Shanghai, China) at 95 °C for 30s, then for 15 s, and after that, at −60 °C for 15 s and 70 °C for 15 s through 40 cycles(Rola et al., 2006). The primers (online resource 13) were synthesized by Sangon Biotech Co., Ltd., Shanghai, China. The relative expression levels of the circRNAs were depicted as $2^{(-\triangle\triangle CT)}$.

2.10. Dual-luciferase reporter gene assay

The 3'-UTR of CXCR2 mRNA, containing putative target sites for mmu-let-7a-5p, was amplified by PCR from genomic DNA. The amplicon was inserted downstream of the luciferase reporter gene in a pMIR-REPORT™ vector according to standard procedures (Promega, Madison, WI, USA). Plasmid DNA was subsequently isolated from recombinant colonies and sequenced to ensure its authenticity. HT22 cells were co-transfected with wild-(pMIR- CXCR2-wt) or mutant-type (pMIR- CXCR2-mt) reporter vectors and let-7a-5p mimic or inhibitor using Lipofectamine 2000 transfection reagent. Cells were collected 36 h after transfection and analyzed using a Dual-Luciferase Reporter Assay System according to the manufacturer's protocol (Promega). All the experiments were performed in triplicate.

2.11. RNA-RNA pull-down assay

HT22 cells were harvested when they reached 70–80% confluence, lysed in buffer with RNase inhibitor and stored in −80 °C for further use. The full-length circRNA chr8_87,859,283–87,904,548 was amplified by PCR from mouse genomic DNA and then inserted into a pGEM-T vector. The recombinant pGEM-T-chr8 plasmids were transfected into bacterials for further amplification. All amplified pGEM-T-chr8 plasmids were collected and cut by DNase I. The correct circRNA chr8_87,859,283–87,904,548 amplicons were purified and labeled with biotin. The biotin-labeled circRNA was further connected with streptomycin affinitive magnetic beads. The magnetic bead complex was then incubated with HT22 cells' lysate, and the pull-down RNA was harvested and purified. The existence of mmu-let-7a-5p was determined by q-PCR.

2.12. ELISA and Western blot analysis

Commercially available ELISA assay kits (#SEA133Mu, #SEA079Mu, USCN Life Science Inc., Wuhan, China) were applied to detect interleukin (IL)-1b and tumor necrosis factor (TNF)-α(Zhong et al., 2017a). Nitrite in the culture media was also measured using the Griess method to assess NO production (Dubovicky et al., 2014). Rabbit anti-CXCR2 antibody (1:500, MAB2164-SP, Bio-Techne China Co. Ltd. Shanghai, China) and mouse anti-GAPDH antibody (1:1000, ab8245, Abcam, Cambridge, UK) were used to conduct Western blotting(Zhong et al., 2017a).

2.13. Recombinant adenovirus, mmu-let-7a-5p mimic and inhibitor

The circRNA chr8_87,859,283–87,904,548-over-expressing recombinant adenovirus ("Ad-cirRNA-Chr-8", 9×10^{10} pfu/mL) and empty carrier adenovirus ("Ad-GFP", 5×10^{10} pfu/mL) (Heyuan Biotechnology Co., Ltd., Shanghai, China) were amplified in human embryonic kidney 293 (HEK293) cells and purified using a Sartorius Vivapure AdenoPACK 20(Guo et al., 2016). The 50% tissue culture infectious dose (TCID50) method was applied to detect viral titers(Guo et al., 2016). The mmu-let-7a-5p mimic and inhibitor were purchased from RiboBio.

(Guangzhou, China). The mimic and inhibitor (2.5 μ g/2.5 μL) were diluted with 1.25 μ l of Entranster TM *in vivo* transfection reagent (Engreen, Beijing, China). The solution was mixed, kept at room temperature for 15 min, and then injected intracerebroventricularly. To transfect cells, the mimic or inhibitor was diluted to a final concentration of 50 ng/μL.

2.14. Intracerebroventricular injection

The adenovirus was diluted to 1.3×10^{10} pfu/mL with enhanced transfection solution(Teng et al., 2016). After achieving an appropriate level of general anesthesia, 3 μL of adenovirus solution were stereotactically injected into the right lateral ventricle of mice at a rate of 0.2 μL/min using a 5-μL-gauge microsyringe at the following stereotactic coordinates (mm from the bregma): AP + 1.5, ML + 1, and DV -2(Donofrio et al., 2006). On the 7th day prior to TBI, the adenovirus was injected, and on the 3rd day prior to TBI, the mimic was injected.

2.15. Measurements of neurological functions

On the 1st, 3rd, 7th and 14th days after TBI, motor function was assessed *via* NSS scoring and the rotarod test. Cued learning on the 15th, 16th, 17th, 18th, 19th, and 20th days and spatial memory on the 21st day after TBI were measured using the Morris water maze test. In the wire grip test, the apparatus consisted of a stainless steel bar (50 cm long; 2 mm in diameter) mounted on two vertical supports and elevated 37 cm above a flat surface (Zhong et al., 2017a; Zhong et al., 2017b). Mice were placed on the bar midway between the supports and were observed for 60 s. In the rotarod test, mice were placed on the rotating rod. The trial ended when the mouse either completed the task (maximum of 2 min), fell completely off the rungs, or gripped the device and spun around for two consecutive revolutions without attempting to walk on the rod (Zhong et al., 2017a; Zhong et al., 2017b). The duration for which mice remained on the rod was recorded, and the mean was the final score. In the Morris water maze test, a submerged platform was placed 1 cm under the water surface, and nontoxic, white pigment was mixed into the water. Each mouse was released from quadrant 1 to 4 once per day and was allotted 90 s to search the hidden platform. The trial ended when the mouse either found the platform and stayed on it for 5 s or did not find the platform within 90 s (Zhong et al., 2017a; Zhong et al., 2017b). Four trials were performed per day for five consecutive days with the location of the platform kept constant. On the last testing day, the platform was removed and the swimming track, dwelling time, and path length in every quadrant were recorded by a computer The assessment was repeated three times on every testing day. All tests were performed by two investigators who were blinded to the experimental grouping.

2.16. Statistical analyses

Statistical analyses were performed using SPSS 20 (Chicago, USA). The results are presented as the mean ± standard deviation (SD). Data from the NSS, rotarod test, and water maze test were analyzed *via* repeated-measures two-way ANOVA, followed by Tukey's *post hoc* test to analyze across the groups(Zhong et al., 2017a). The remaining data were analyzed *via* Student's *t*-test or randomized one-way ANOVA, followed by Tukey's *post hoc* test to carry out the group comparisons (Zhong et al., 2017a). The value $P < .05$ was accepted as statistically significant.

3. Results

3.1. The identification of circRNAs in each sample

All the valid sequencing data were submitted to the GEO database (ID: GSE79441) (Zhong et al., 2016). A large amount of circRNAs were discovered in the mouse cerebral cortex. For each circRNA, the name of its derived gene, chromosome orientation, strand location, and starting and ending sites, as well as its fold change were shown in Online resource 1–6 and Table 1. For example: in the Normal 1 sample, a total of 12,582 circRNAs were discovered (Online resource 1). Among these circRNAs, 6237 were aligned to the positive (+) strand and 6345 were aligned to the negative (−) strand (Fig. 1, A). The location of all 12,582 circRNAs were differentially distributed into the mouse chromosomes (Fig. 1, B). CircRNA can be derived from the exons of coding genes, and the 3-exons-spread was the most common type of circRNA in the Normal 1 sample (Fig. 1, C). In addition, the volcano plots of the

Table 1
Circular RNA (circRNA) distribution in each sample.

Sample	Total circRNA	Strand (+)	Strand (−)	Most popular type	Chromosome distribution
Normal 1	12,528	6237	6345	3-exons-spread	all
Normal 2	13,565	6808	6757	3-exons-spread	all
Normal 3	14,834	7399	7435	3-exons-spread	all
TBI 1	13,574	6797	6777	3-exons-spread	all
TBI 2	14,534	7263	7271	3-exons-spread	all
TBI 3	12,256	6047	6209	3-exons-spread	all

expression profile for all the identified circRNAs were shown in Fig. 2A.

3.2. The differentially expressed circRNA in the traumatic cerebral penumbra cortex after TBI

In the present study, a total of 8036 circRNAs were altered in the mouse cerebral cortex after TBI (Online resource 7). A detailed description, including their chromosome location, starting and ending sites, overlapping among the 6 samples, fold changes and FDR were shown in Online resource 7. Among the 8036 altered circRNAs, a total of 16 circRNAs were significantly changed based on the filter rule [$|\log_2^{(\text{fold change})}| > 1$, $P < .05$ and FDR < 0.05] and shown in Fig. 2A-B and Table 2 (5 up-regulated and 11 down-regulated).

3.3. Validation of circRNAs expression by RT-PCR

To validate the reliability of circRNA sequencing, five random circRNAs (Online resource 8) were selected to perform RT-PCR. The circRNA expression detected by RT-PCR was consistent with that measured by the RNA-seq (Fig. 2C). This validation indicated the good reproducibility and reliability of the RNA-seq and circRNA calculation.

3.4. The GO and KEGG analyses of circRNA-derived genes

The possible functions of circRNA may be related to their derived genes. To predict the possible functions of circRNA, the circRNA-derived genes were subjected to GO and KEGG analyses. A total of 287 GO

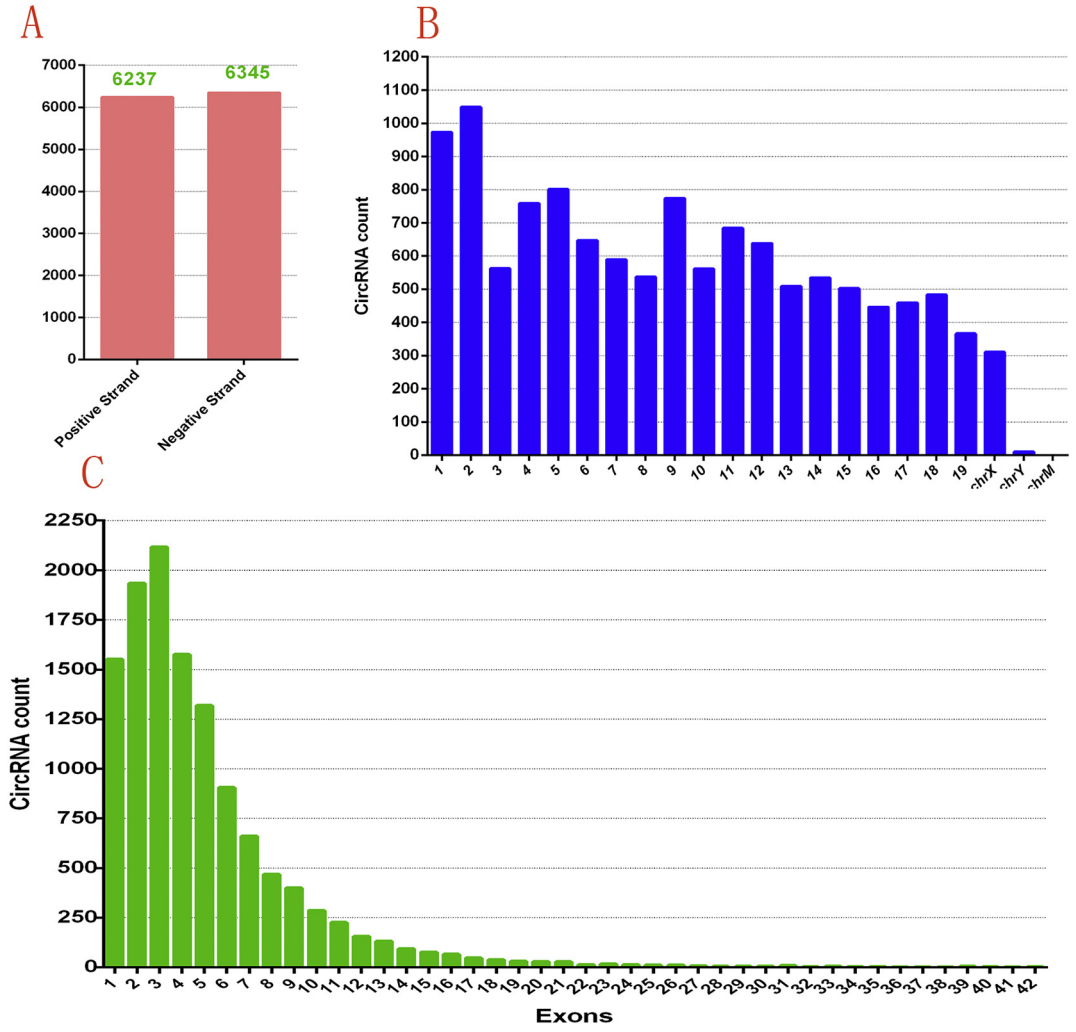

Fig. 1. Strand location, chromosome orientation and exons-spread type of circRNA in the "Normal 1" sample (n = 18). (A) The strand location of all circRNA genes. The "+" means the positive-sense strand, and the "-" means the anti-sense strand. (B) The chromosome orientation of all circRNA. The horizontal axis is the chromosome number, and the vertical axis is the circRNA count. (C) The exons-spread type of circRNA. The horizontal axis is the exon count, and the vertical axis is the circRNA count.

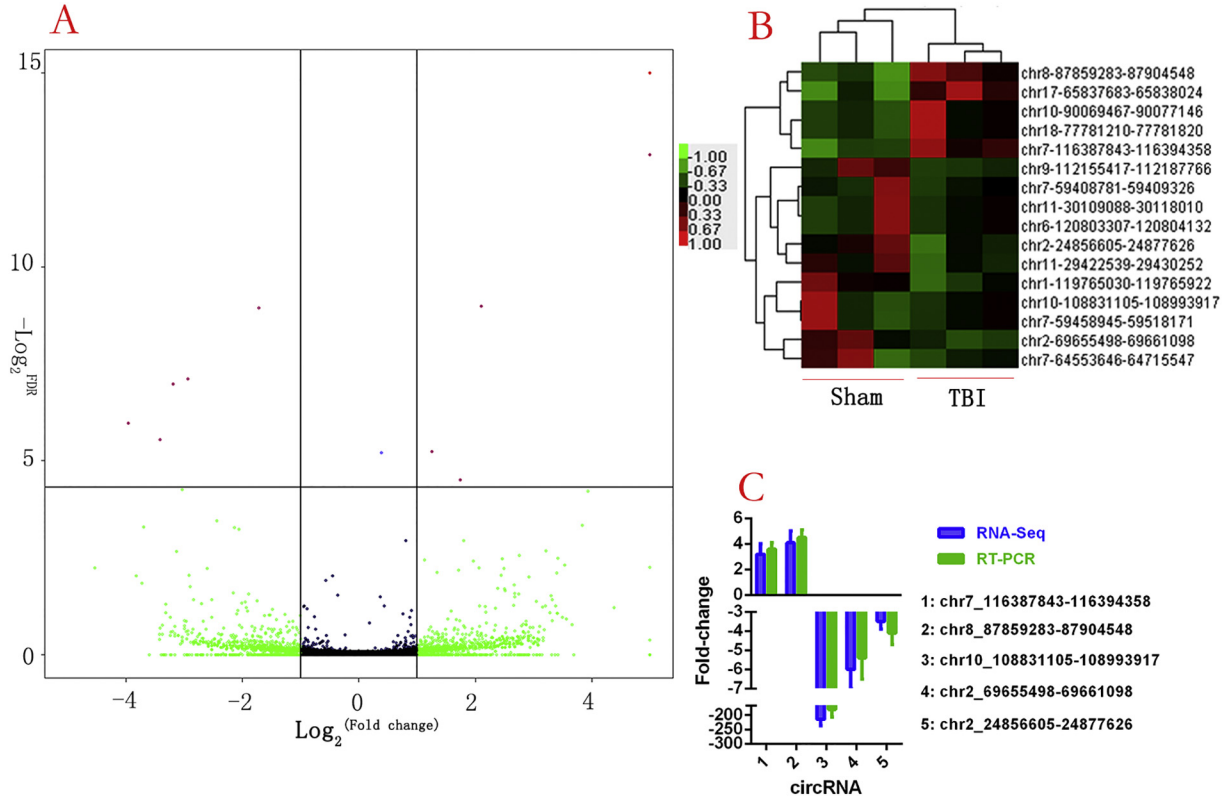

Fig. 2. Volcano plots, heat map and RT-PCR results of circRNA (n = 18). (A) The volcano plots of all the detected circRNA in both the normal and the TBI groups. The red plots represent significantly changed circRNAs with > 2.0-fold-change and corrected P value < .05. (B) The heat map of the 16 significantly changed circRNAs. Data normalized by Z score transformation were used in the calculation of significant changes in circRNA expression, and the transformed data were used to construct the heat map. (C) The comparison of the respective results from RNA-seq and RT-PCR to verify the reliability of the RNA-seq technique.

terms (Online resource 9) and 103 KEGG pathways (Online resource 10) were figured out according to the following criteria: $P < .05$ and FDR < 0.05. The top 20 biological processes (BP), top 20 molecular functions (MF) and top 20 cellular components (CC) were shown in Figs. 3A-C. Additionally, the top 20 pathways were shown in Fig. 3D. The analyses suggested that circRNA might be involved in several processes and networks, including neuroinflammation, axon guidance, synapses.

3.5. The target miRNA prediction of the significantly changed circRNAs and the regulating network

In present study, one circRNA potentially captured several miRNAs. On the other hand, one miRNA could be arrested by several circRNAs. The detailed prediction is shown in Online resource 11 and Table 3. The significant mRNA alteration in the cerebral cortex after TBI was measured in our previous study(Zhong et al., 2016), the target miRNA prediction of mRNA was also calculated in the present study (Online resource 12, Table 4). It was found that some miRNAs could be competitively captured by both circRNA and mRNA, suggesting that circRNA may regulate mRNA through sequestering their common competitive miRNAs. The reciprocally regulating network was shown in Online resource 13.

Table 2
The significantly changed circRNAs after TBI.

CircRNA	Normal RPKM	TBI RPKM	Style	$Log_2^{(Fold\ change)}$	Gene Length
chr7–116,387,843-116,394,358	5.57	18.60	up	1.74	6515 bp
chr17–65,837,683-65,838,024	13.00	30.89	up	1.25	341 bp
chr8–87,859,283-87,904,548	6.02	25.94	up	2.10	45,265 bp
chr10–90,069,467-90,077,146	0	37.54	up	20	7679 bp
chr18–77,781,210-77,781,820	0	87.60	up	20	610 bp
chr1–119,765,030-119,765,922	9.10	0.85	down	−3.42	892 bp
chr9–112,155,417-112,187,766	8.87	0.57	down	−3.96	32,349 bp
chr11–29,422,539-29,430,252	12.51	1.37	down	−3.20	7713 bp
chr2–69,655,498-69,661,098	13.08	1.71	down	−2.94	5600 bp
chr2–24,856,605-24,877,626	25.71	7.79	down	−1.72	21,021 bp
chr10–108,831,105-108,993,917	215.64	1.02	down	−7.72	162,812 bp
chr7–64,553,646-64,715,547	58.02	0	down	−20	161,901 bp
chr6–120,803,307-120,804,132	93.29	0	down	−20	825 bp
chr7–59,458,945-59,518,171	64.50	0	down	−20	59,226 bp
chr11–30,109,088-30,118,010	59.73	0	down	−20	8922 bp
chr7–59,408,781-59,409,326	71.16	0	down	−20	545 bp

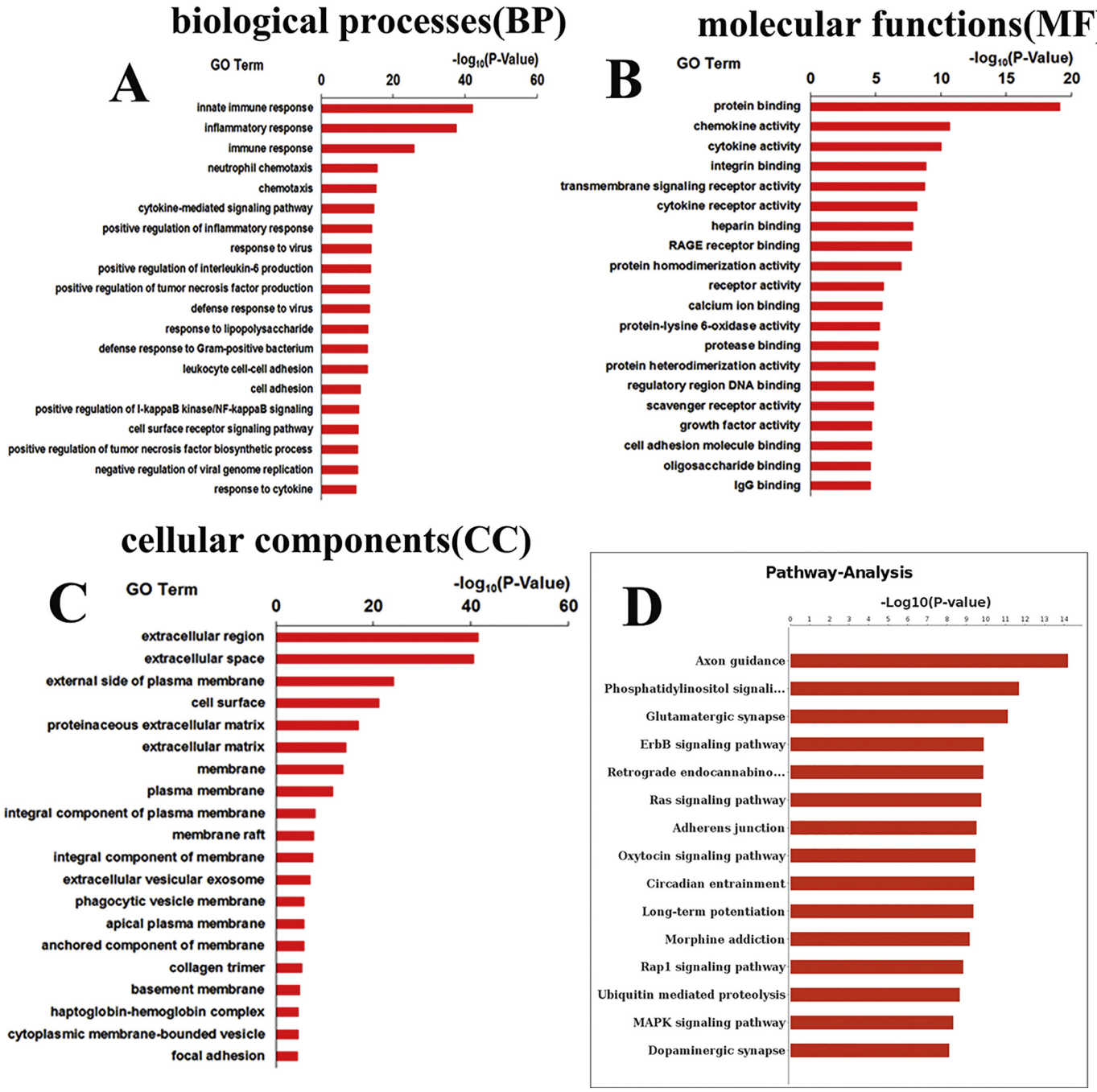

Fig. 3. KEGG and GO analyses of all changed circRNA (n = 18). The GO terms and KEGG pathways were figured out according to the rule: $P < 0.05$ and FDR < 0.05. (A) The top 20 biological processes. (B) The top 20 molecular functions. (C) The top 20 cellular components. (D) The top 20 pathways. The horizontal axis is the "$-\log_{10}{}^{(p\text{-value})}$", and the vertical axis is the name of the GO terms or pathways.

3.6. CircRNA chr8_87859283-87904548 regulated CXCR2 by sponging mmu-let-7a-5p

CircRNA chr8_87859283-87904548 was 261 bp and significantly increased in the mouse cerebral cortex after TBI ($P < .05$, Fig. 4A). The aforementioned regulating network suggested that mmu-let-7a-5p might be competitively captured by both circRNA chr8_87859283-87904548 and the mRNA of the C-X-C chemokine receptor type 2 (CXCR2) gene (Online resource 13). Therefore, we hypothesized that circRNA chr8_87859283-87904548 might regulate the CXCR2 mRNA by competitively sequestering mmu-let-7a-5p. A series of experiments were performed to verify this regulating mechanism between chr8_87859283-87904548 and CXCR2.

3.6.1. 1CXCR2 was regulated by mmu-let-7a-5p

In the dual-luciferase reporter gene assay, the recombinant CXCR2–3'UTR plasmids, including either the wild-type or mutant-type binding site of mmu-let-7a-5p, were treated with miRNA mimic or inhibitor. Compared to the CXCR2-Wt + Nc group (125.00 ± 21.00), the relative F-luc/R-luc ratio was significantly decreased in the CXCR2-Wt + Mimic group (35.00 ± 9.00), but significantly increased in the CXCR2-Wt + Inhibitor group (208.00 ± 35.00) ($P < .05$, Fig. 4B). When the binding site of mmu-let-7a-5p was mutated, the F-luc/R-luc ratio was kept at a relatively high level in both the CXCR2-Mut + Mimic group (274.00 ± 49.00) and CXCR2-Mut + inhibitor group (281.00 ± 58.00), and neither the mimic nor the inhibitor influenced the ratio ($P > .05$, Fig. 4B).

Table 3
Targeting microRNA (miRNA) prediction of the significantly changed circRNAs.

circRNA		miRNA			
Name	$Log_2^{(fold\text{-}change\text{-}circRNA)}$	Number	Example	Binding site (Start)	Binding site (End)
chr7–116,387,843-116,394,358	1.74	166	mmu-miR-138-5p	3390	4010
chr17_65,837,683_65,838,024	1.25	11	mmu-miR-140-3p	136	158
chr8–87,859,283-87,904,548	2.10	786	mmu-let-7 g-3p	39,624	39,646
chr10–90,069,467-90,077,146	20	134	mmu-miR-138-2-3p	5714	5733
chr18–77,781,210-77,781,820	20	16	mmu-miR-761	163	181
chr1–119,765,030-119,765,922	−3.42	9	mmu-miR-181b-5p	590	616
chr9–112,155,417-112,187,766	−3.96	549	mmu-let-7 g-5p	14,434	14,455
chr11–29,422,539-29,430,252	−3.20	128	mmu-miR-15b-5p	3264	3284
chr2–69,655,498-69,661,098	−2.94	220	mmu-miR-15b-5p	4543	4567
chr2–24,856,605-24,877,626	−1.72	64	mmu-miR-29b-3p	5656	5680
chr10–108,831,105-108,993,917	−7.72	968	mmu-let-7 g-5p	142,298	142,319
chr7–64,553,646-64,715,547	−20	1046	mmu-miR-23b-3p	55,117	55,138
chr6–120,803,307-120,804,132	−20	28	mmu-miR-150-3p	747	768
chr7–59,458,945-59,518,171	−20	309	mmu-miR-99b-5p	18,732	18,754
chr11–30,109,088-30,118,010	−20	295	mmu-miR-23b-5p	7135	7156
chr7–59,408,781-59,409,326	−20	26	mmu-miR-24-3p	90	108

To further verify the effect of mmu-let-7a-5p on CXCR2-mRNA, the CXCR2 protein was assessed by Western blotting when cells were treated with either the mimic or inhibitor. The CXCR2 protein level was significantly raised when cells were treated with the mmu-let-7a-5p inhibitor but significantly reduced when treated with the mimic ($P < .05$, Fig. 4C-D). These data suggest that mmu-let-7a-5p could bind with the 3'UTR of CXCR2-mRNA to hinder its translation.

3.6.2. mmu-let-7a-5p was pulled down by circRNA chr8_87859283-87904548

Our network analysis predicted the complementary combination between mmu-let-7a-5p and circRNA chr8_87859283-87904548. An RNA-RNA pull-down assay was carried out to explore the combination. Compared to the antisense group (0.05 ± 0.02), the mmu-let-7a-5p level was significantly higher in the circRNA-Chr-8 group (0.74 ± 0.09) and highest in Input group (1.00 + 0.15) ($P < .05$, Fig. 4E), suggesting that mmu-let-7a-5p could be pulled down by circRNA chr8_87,859,283–87,904,548.

3.6.3. CXCR2 was regulated by circRNA chr8_87859283-87904548

CircRNA can function as a miRNA sponge and isolator (Hansen et al., 2013). Therefore, we hypothesized that circRNA chr8_87859283-87904548 might weaken the inhibiting effect of mmu-let-7a-5p on CXCR2-mRNA, resulting in increased production of the CXCR2 protein. In HT22 cells, when compared to the Ad-GFP group, the CXCR2 protein was significantly increased in the Ad-cirRNA-Chr-8 group ($P < .05$, Fig. 4F-G). In the cerebral cortex of C57BL/6 mice, the CXCR2 protein was significantly increased in the Ad-cirRNA-Chr-8 group when compared to Ad-GFP group, but this increase was partially reversed by mimic treatment in the Ad-cirRNA-Chr-8 + mimic group ($P < .05$, Fig. 4H—I). In C57BL/6 mice, the circRNA chr8_87859283-87904548 level was significantly raised in the traumatic cerebral penumbra cortex on the 1st, 3rd, and 7th days after TBI when compared with its pre-TBI level ($P < .05$, Fig. 4A). Similarly, the CXCR2 protein in the traumatic cortex was also significantly increased on the 1st, 3rd, and 7th days after TBI ($P < .05$, Fig. 4 J-K). These data suggest a potential promoting role of the over-expression of circRNA chr8_87859283-87904548 for producing more CXCR2 protein.

3.7. Over-expression of circRNA chr8_87859283-87904548 promoted more production of inflammatory cytokines

3.7.1. The in vitro pro-inflammatory effect of circRNA chr8_87859283-87904548

CXCR2 has been found to promote acute inflammation(Bajrami et al., 2016a; Marchelletta et al., 2015; Wu et al., 2015a). Since circRNA chr8_87,859,283–87,904,548 promoted more CXCR2 protein production, we hypothesized that circRNA chr8_87,859,283–87,904,548 might play a pro-inflammatory role. ELISA was conducted to measure the concentrations of inflammatory cytokines in BV2 cells. LPS induced a significant increase of IL-1b (381.00 ± 48.00), TNF-α (493.00 ± 89.00) and NO level (63.00 ± 10.00) when compared to its counterpart in the Non-treated group (53.00 ± 11.00; 39.00 ± 8.00; 5.00 ± 2.00) ($P < .05$, Fig. 5A-C), and this increase was further augmented by Ad-cirRNA-Chr-8 treatment. The concentration of IL-1b (603.00 ± 65.00) and TNF-α (962.00 ± 113.00) in the Ad-cirRNA-Chr-8 + LPS group were significantly higher than that in the Ad-GFP + LPS group (387.00 ± 55.00; 504.00 ± 96.00)

Table 4
Targeting miRNA prediction of the top 10 significantly changed mRNAs.

mRNA		miRNA			
Name	$Log_2^{(fold\text{-}change\text{-}mRNA)}$	Number	Example	Binding site (Start)	Binding site (End)
Tgm1	8.95	3	mmu-miR-3090-3p	97	116
Niacr1	7.86	39	mmu-miR-292a-5p	269	293
Clec4d	8.48	31	mmu-miR-466n-5p	197	218
F10	7.45	60	mmu-miR-1191b-3p	234	255
Slfn4	7.68	6	mmu-miR-383-5p	689	709
Cxcr2	7.74	12	mmu-miR-6961-3p	104	125
Il1f9	7.62	21	mmu-miR-504-3p	692	713
Cxcl3	8.85	2	mmu-miR-466c-5p	376	399
Mefv	8.29	15	mmu-miR-6990-5p	59	80
Gp49a	7.96	5	mmu-miR-697	29	51

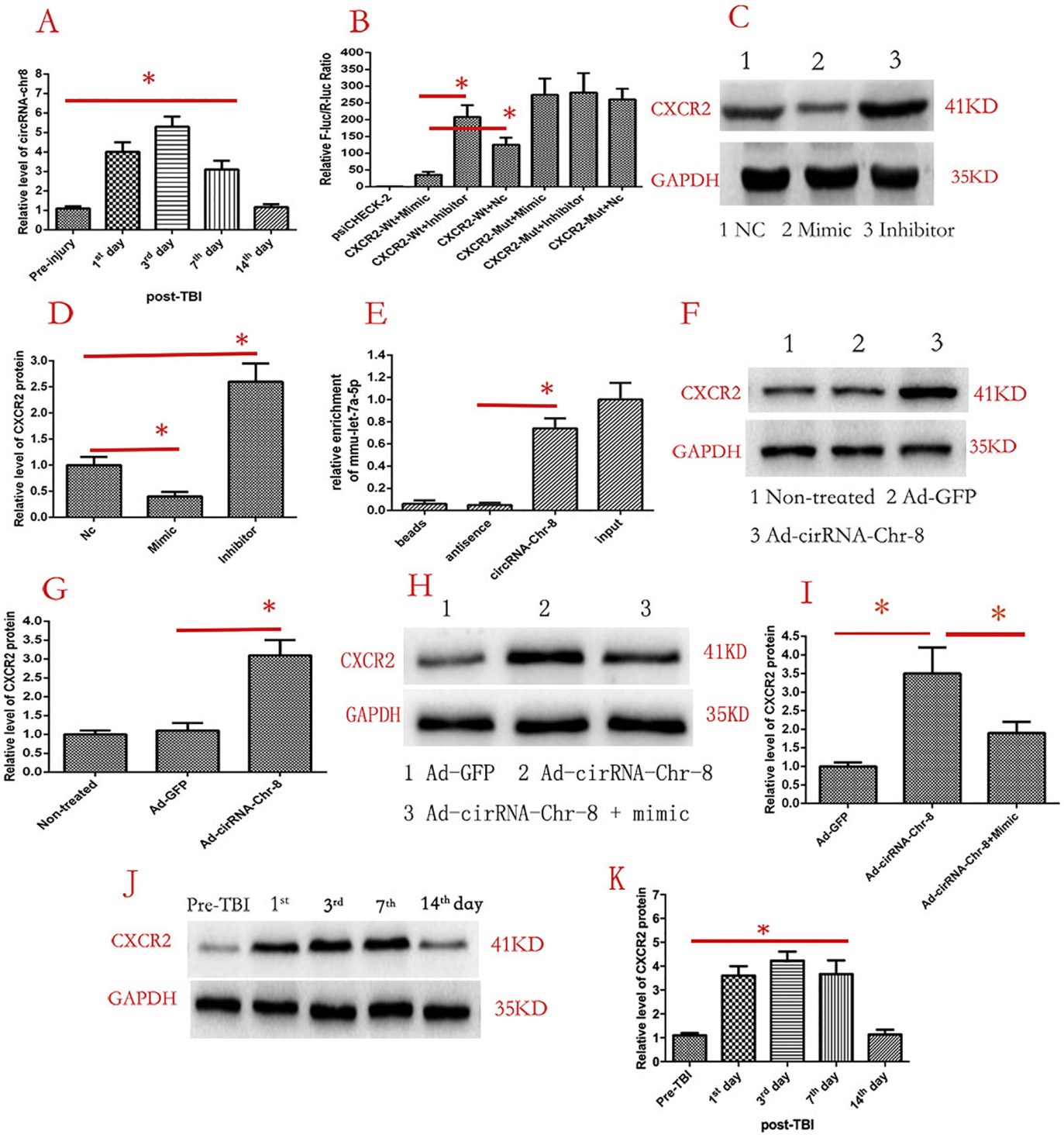

Fig. 4. CircRNA chr8_87,859,283–87,904,548 (circRNA-chr-8) regulates CXCR2 protein level through sequestering mmu-let-7a-5p. (A) The circRNA-chr-8 level in mouse cerebral cortex after TBI (n = 25). (B) The impact of mmu-let-7a-5p on the recombinant CXCR2–3'UTR plasmids. "F-luc/R-luc": the ratio of the firefly/renilla luciferase activities; "psiCHECK-2" is the empty plasmid; "mimic" or "inhibitor": mimetic or inhibitor of mmu-let-7a-5p. (C-D) Western blot assay to measure the effect of mmu-let-7a-5p on the CXCR2 protein level. (E) The respective mmu-let-7a-5p level under different pull-down conditions ("beads": blank control; "antisense": the non-specific RNA chain with 261 bp length; "circRNA-chr-8": the whole-length circRNA chain). (F—I) Western blot assay to measure the effect of circRNA-chr-8 adenovirus on the CXCR2 protein level in HT22 cells and mouse cerebral cortex (n = 15). (J-K) The CXCR2 protein level in the mouse cerebral cortex after TBI (n = 25). All the data are expressed as the mean ± SD; one-way ANOVA with Tukey's *post hoc* test and students' T-test; *p < .05. All experiments were repeated 3 times.

(P < .05, Fig. 5A-B). Similarly, the NO level was also significantly higher in the Ad-cirRNA-Chr-8 + LPS group (104.00 ± 16.00) than in the Ad-GFP + LPS group (66.00 ± 13.00) (P < .05, Fig. 5C), indicating an *in vitro* pro-inflammatory effect of circRNA chr8_87,859,283–87,904,548; however, the Ad-cirRNA-Chr-8 treatment alone without LPS did not significantly increase IL-1b (70.00 ± 13.00), TNF-α (60.00 ± 16.00) and NO level (9.00 ± 5.00) when compared to the Non-treated group (53.00 ± 11.00;

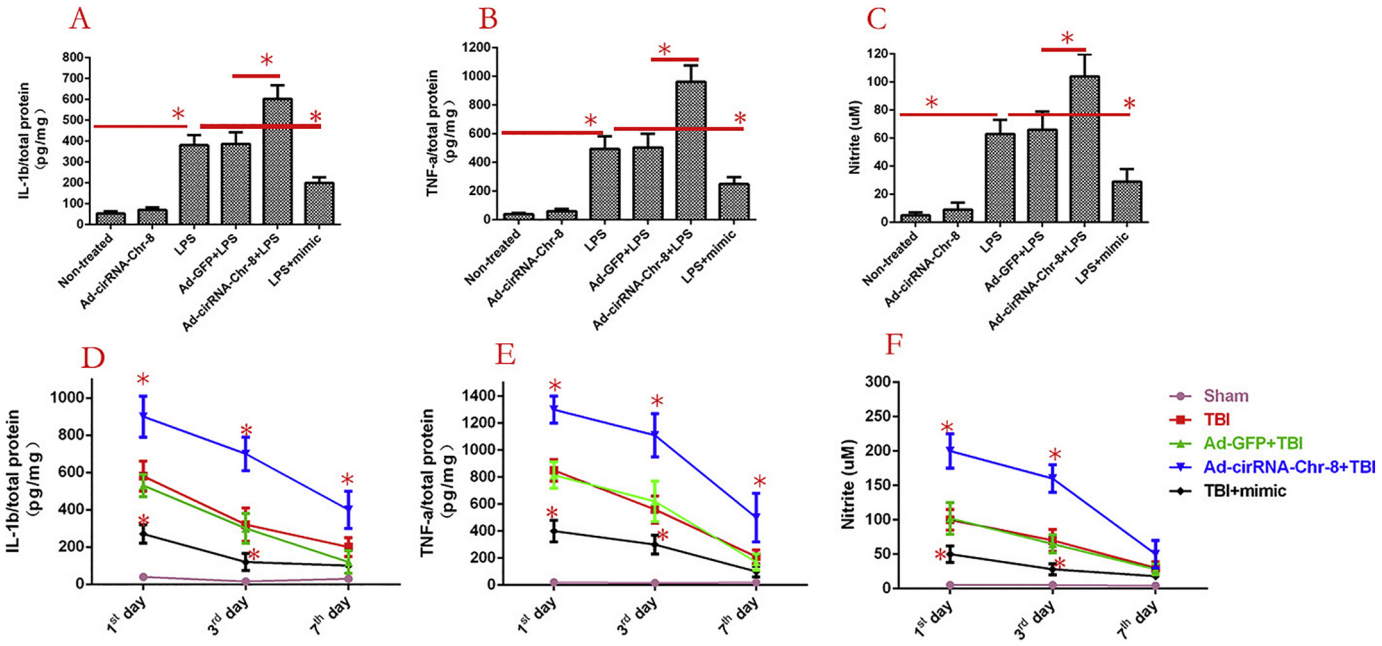

Fig. 5. *In vitro* and *in vivo* pro-inflammatory effects of circRNA-chr-8. ELISA was conducted to measure the levels of inflammatory cytokines. (A-C) The respective level of IL-1b, TNF-αand NO in differently treated BV-2 cells. "Ad-cirRNA-Chr8": the adenovirus to over-express circRNA-chr-8; "LPS": lipopolysaccharide; "mimic": mimetic of mmu-let-7a-5p. (D-F) The respective level of IL-1b, TNF-αand NO in mouse cerebral cortex around the injury focus after TBI (n = 65). All the data are expressed as the mean ± SD; one-way ANOVA with Tukey's *post hoc* test and students' t-test; *p < .05. All experiments were repeated 3 times.

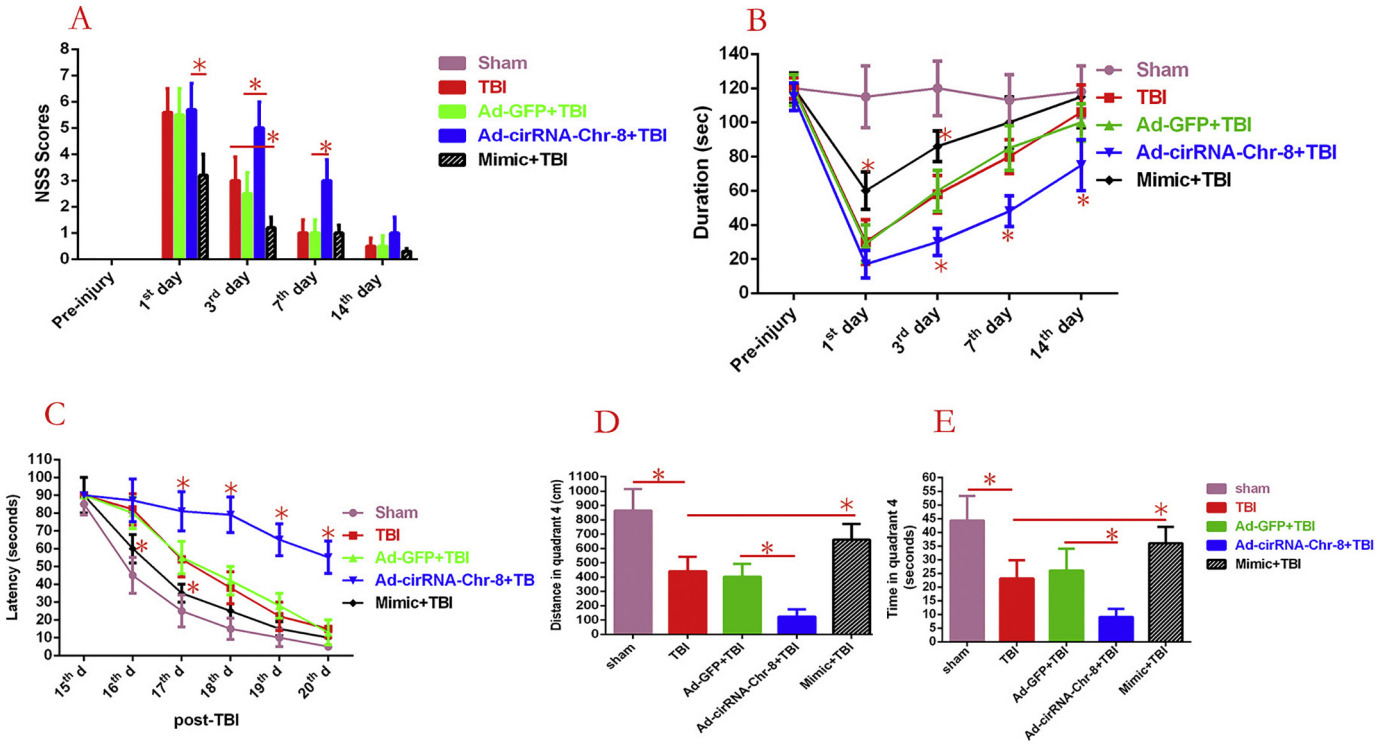

Fig. 6. CircRNA-chr-8 inhibits the restoration of motor and cognitive function in mice after TBI (n = 25). (A) NSS scores. (B) Duration in the rotarod test. (C) Latency to locate the hidden platform. (D) Length of the swimming tracks in quadrant 4, where the platform was originally located. (E) Dwelling time in quadrant 4. "Ad-cirRNA-Chr8": the adenovirus to over-express circRNA-chr-8; "mimic": mimetic of mmu-let-7a-5p. Repeated-measures two-way ANOVA with Tukey's *post hoc* test; *p < .05. All tests were performed by two blind observers.

39.00 ± 8.00; 5.00 ± 2.00) (P > .05, Fig. 5A-C). Moreover, the LPS-induced increase of IL-1b (381.00 ± 48.00), TNF-α (493.00 ± 89.00) and NO level (63.00 ± 10.00) was significantly reversed by mmu-let-7a-5p mimic treatment (200.00 ± 26.00; 249.00 ± 43.00; 29.00 ± 9.00) (P < .05, Fig. 5A-C).

3.7.2. The in vivo pro-inflammatory effect of circRNA chr8_87859283-87904548

TBI induced a significant increase of IL-1b, TNF-α and NO level when compared to the sham group (P < .05, Fig. 5D-F), and this increase of inflammatory cytokines was further augmented by Ad-

cirRNA-Chr-8 treatment. The concentration of IL-1b in the Ad-cirRNA-Chr-8 + TBI group (879.00 ± 103.00; 714.00 ± 91.00; 398.00 ± 97.00) were significantly higher than that in the Ad-GFP + TBI group (531.00 ± 68.00; 275.00 ± 85.00; 126.00 ± 68.00) on the 1st, 3rd, and 7th days after TBI ($P < .05$, Fig. 5D). Similarly, the concentration of TNF-α in the Ad-cirRNA-Chr-8 + TBI group (1312.00 ± 179.00; 1110.00 ± 148.00; 508.00 ± 87.00) were significantly higher than that in the Ad-GFP + TBI group (815.00 ± 97.00; 620.00 ± 93.00; 177.00 ± 51.00) on the 1st, 3rd, and 7th days after TBI ($P < .05$, Fig. 5E). Moreover, the NO level in the Ad-cirRNA-Chr-8 + TBI group (202.00 ± 38.00; 161.00 ± 33.00) were significantly higher than that in the Ad-GFP + TBI group (104.00 ± 23.00; 65.00 ± 11.00) on the 1st and 3rd days after TBI ($P < .05$, Fig. 5F). These data suggest an *in vivo* pro-inflammatory effect of circRNA chr8_87,859,283–87,904,548. In addition, all of these TBI-induced increases of inflammatory cytokines were partially relieved by mmu-let-7a-5p mimic treatment on the 1st and 3rd days after TBI (P < .05, Fig. 5D-F).

3.8. The over-expression of circRNA chr8_87859283-87904548 blocked the restoration of neurological function after TBI in C57BL/6 mice

To determine the influence of circRNA chr8_87,859,283–87,904,548 on the recovery of the neurological functions of mice following TBI, the NSS test, rotarod test and water maze test were conducted to assess the motor function, learning ability and spatial memory, respectively. On the 3rd and 7th day after TBI, the NSS scores of the Ad-cirRNA-Chr-8 + TBI group (5.50 ± 1.20; 3.50 ± 0.60) was significantly higher than that of the Ad-GFP group (2.50 ± 0.80; 1.00 ± 0.40) ($P < .05$, Fig. 6A). On the 1st and 3rd day after TBI, the NSS scores of the mimic + TBI group (3.20 ± 0.80; 1.20 ± 0.40) was significantly lower than that of the TBI group (5.60 ± 0.90; 3.00 ± 0.70) ($P < .05$, Fig. 6A). Furthermore, on the 3rd, 7th and 14th day after TBI, the duration of the Ad-cirRNA-Chr-8 + TBI group in the rotarod test (30.00 ± 8.00s; 48.00 ± 9.00s; 65.00 ± 13.00s) was significantly shorter than that of the Ad-GFP + TBI group (63.00 ± 10.00s; 85.00 ± 14.00s; 100.00 ± 11.00s) ($P < .05$, Fig. 6B), indicating a worse motor function in the Ad-cirRNA-Chr-8 + TBI group. On the 1st and 3rd day after TBI, the duration of the mimic + TBI group in the rotarod test (60.00 ± 10.00; 86.00 ± 12.00) was significantly longer than that of the TBI group (30.00 ± 11.00; 55.00 ± 12.00) ($P < .05$, Fig. 6B). On the 17 th, 18 th, 19 th and 20th days after TBI, in water maze test, the latency of the Ad-cirRNA-Chr-8 + TBI group to find the hidden platform (81.00 ± 11.00s; 79.00 ± 12.00s; 65.50 ± 9.00s; 55.50 ± 11.00s) was significantly longer than that of the Ad-GFP + TBI group (51.00 ± 13.00 s; 42.00 ± 8.00 s; 28.00 ± 7.00 s; 13.00 ± 5.00 s) ($P < .05$, Fig. 6C), indicating a worse learning ability of the Ad-cirRNA-Chr-8 + TBI group. On the 16 th and 17 th day after TBI, the latency of the mimic + TBI group (60.00 ± 8.00 s; 33.00 ± 5.00 s) was significantly shorter than that of the TBI group (82.50 ± 9.00 s; 54.00 ± 10.00 s) ($P < .05$, Fig. 6C). On the last testing day (21st day after TBI, the hidden platform was removed), the swimming track of the Ad-cirRNA-Chr-8 + TBI group (123.05 ± 52.00 cm) in quadrant 4, − where the original platform was located,- was significantly shorter than that of theAd-GFP + TBI group (402.00 ± 99.50 cm) ($P < .05$, Fig. 6D). The swimming track of the mimic + TBI group (661.00 ± 99.00 cm) was significantly longer than that of the TBI group (435.00 ± 89.50 cm) ($P < .05$, Fig. 6D). Similarly, the dwelling time of the Ad-cirRNA-Chr-8 + TBI group (9.05 ± 3.00 s) spent in quadrant 4 was also significantly shorter than that of the Ad-GFP + TBI group (26.00 ± 8.00 s), indicating a worse memory of the Ad-cirRNA-Chr-8 + TBI group (P < .05, Fig. 6E). The dwelling time of the mimic + TBI group (36.00 ± 6.00 cm) was significantly longer than that of the TBI group (21.00 ± 5.50 cm) (P < .05, Fig. 6D). These data suggest an inhibitory effect of circRNA chr8_87,859,283–87,904,548 on neurological restoration following TBI.

4. Discussion

CircRNA has been recently discovered as a new member of endogenous, non-coding RNA. CircRNA has neither 5′–3′ polarities nor polyadenylated tails and forms covalently closed-loop structure (Qu et al., 2015), resulting in its stable specialty. CircRNA is endogenous, relatively abundant, and conserved in mammalian cells (Qu et al., 2015). CircRNA has been reported to be involved in CNS diseases, such as glioma (Song et al., 2016), Alzheimer's disease (Lukiw, 2013), and in brain development (Veno et al., 2015), as well as OGD/R-induced neuronal injury (Lin et al., 2016). TBI remains a severe acute CNS disease, and the complex mechanism of secondary brain damage following TBI still needs to be elucidated. Therefore, we presently used deep RNA-Seq to draw the circRNA atlas in traumatic cerebral penumbra cortex following TBI.

A total of 16 circRNAs were discovered to significantly change after TBI in our present sequencing study. Unfortunately, it is difficult to elucidate their exact functions. CircRNA molecules are transcribed and spliced from the exons of host genes, which they may possibly influence (Salzman, 2016). CircRNA can regulate the alternative splicing and modulate the expression of host genes through acting as a miRNA sponge (Memczak et al., 2013; Zhang et al., 2013; Li et al., 2015). Therefore, we carried out KEGG and GO analyses for host genes and showed that the significantly changed circRNAs may be involved in many important pathways, such as the Ras signaling pathway, oxytocin signaling pathway and MAPK signaling pathway. These pathways suggest non-negligible roles of circRNA in secondary injury and neuronal repairing following TBI.

MicroRNA is a type of short (18–22 bp) non-coding RNA that can bind to the 3'-UTR of mRNA to inhibit its translation (Hu et al., 2015; Huang et al., 2016; Zhou et al., 2016). CircRNA can act as a sponge to sequester miRNA (Memczak et al., 2013; Zhang et al., 2013; Li et al., 2015). If circRNA and mRNA simultaneously hold the binding sequence for a special miRNA, the circRNA and the mRNA will competitively capture the same miRNA. Moreover, if the circRNA is significantly increased, more miRNA will be captured by circRNA, and less miRNA can bind to mRNA, resulting in more active translation and more protein production, and *vice versa*. Therefore, the altered expression of circRNA may regulate translation and protein production through competitively capturing miRNA. In the present study, the significantly altered expression of many circRNAs were figured out, and the reciprocally regulating network between the changed circRNAs and mRNAs was constructed based on their intermediary miRNAs. The network analysis predicted that circRNA chr8_87,859,283–87,904,548, which was significantly increased approximately 4 times after TBI, may competitively capture miRNA mmu-let-7a-5p with CXCR2-mRNA, resulting in more CXCR2 protein production. Subsequently, we first confirmed the combination of mmu-let-7a-5p with the 3'UTR of CXCR2-mRNA and its inhibiting effect on CXCR2 translation in the dual-luciferase reporter gene assay. Secondly, we confirmed the combination of mmu-let-7a-5p with circRNA chr8_87859283-87904548 in an RNA-RNA pull-down assay. Thirdly, the CXCR2 protein was significantly increased by over-expressing circRNA using an adenovirus, but this increase was reversed by an mmu-let-7a-5p mimic. These results verify our hypothesis that circRNA chr8_87859283-87904548 competitively captures mmu-let-7a-5p to produce more CXCR2 protein. Interestingly, the increased CXCR2 was only partially, not absolutely reversed by mmu-let-7a-5p mimic treatment, indicating that some unrecognized factors may be involved in the regulating process of chr8_87859283-87904548.

CXCR2 is known as a high affinity interleukin-8 (IL-8) receptor, which has been reported to rapidly mobilize neutrophils during early stages of acute inflammation (Bajrami et al., 2016a; Marchelletta et al., 2015). Moreover, CXCR2 plays an essential role in cerebral endothelial

activation and subsequent leukocyte recruitment during neuroinflammation (Wu et al., 2015a). CXCR2 also has been reported to be involved in inflammatory diseases, such as lung inflammation (Tiwari et al., 2016; Lerner et al., 2016), pancreatic inflammation (Steele et al., 2015), skin inflammation (Hsieh et al., 2014) and kidney inflammation (Ranganathan et al., 2013). The expression of circRNA chr8_87,859,283–87,904,548 remained at a high level for a long time after TBI, leading to increased production of CXCR2 protein in the traumatic cerebral cortex. Therefore, we inferred that circRNA might promote inflammatory reaction in the acute phase after TBI. Indeed, when circRNA chr8_87,859,283–87,904,548 was specially up-regulated by adenovirus, the concentration of inflammatory cytokines in traumatic cerebral cortex or in LPS-irritated BV-2 cells was significantly elevated, suggesting its pro-inflammatory role. Moreover, those increased inflammatory cytokines were partially decreased by mmu-let-7a-5p mimic treatment, which further verified the mediating role of mmu-let-7a-5p in the regulating network of circRNA chr8_87,859,283–87,904,548. Interestingly, Ad-cirRNA-Chr-8 treatment alone without LPS did significantly up-regulate CXCR2, but did not significantly increase the inflammatory cytokines in non-irritated BV2 cells. CXCR2 protein is a receptor for IL-8 and chemokine (C-X-C motif) ligand 1 (CXCL1) (Bajrami et al., 2016b; Wu et al., 2015b). It binds to IL-8 or CXCL1 with high affinity and transduces the signal through a G-protein-activated second messenger system (Bajrami et al., 2016b; Wu et al., 2015b). The CXCR2 receptor is able to promote the inflammatory reaction only when it can bind the ligand. When treated with LPS, the BV-2 cells can secrete CXCL1 (Wu et al., 2015b), which can bind with CXCR2 and result in increased production of inflammatory cytokines. In this inflammatory process, CXCR2 is a promoter, but not an initiator. Hence, the Ad-cirRNA-Chr-8 treatment can facilitate the increased production of inflammatory cytokines only in irritated BV-2 cells, but not in resting cells. After TBI, many chemical and physical factors initiate the inflammatory reaction, and in this study, the more CXCR2 protein produced, the more inflammatory cytokines produced. Neuroinflammation is considered one of the most important factors to aggravate secondary brain injury and exacerbate the functional deficit after TBI (Corps et al., 2015; Cederberg and Siesjo, 2010). Hence, we hypothesized that the increased circRNA chr8_87,859,283–87,904,548 after TBI may obstruct neurological restoration. Indeed, when circRNA chr8_87,859,283–87,904,548 was increased by adenovirus in mouse brain, the performances of the Ad-cirRNA-Chr-8 + TBI groupin the NSS, rotarod test and water maze test were worse than that in the Ad-GFP + TBI group, indicating that the elevated circRNA chr8_87,859,283–87,904,548 was not beneficial to the restoration of motor and memorial function after TBI.

Non-coding RNA consists of several major classes, including miRNA, lncRNA and circRNA. The changes of miRNA expression in the contusional cerebral cortex (Lei et al., 2009), hippocampus (Liu et al., 2014) and serum (Sharma et al., 2014) have been previously reported. Additionally, the altered lncRNA expression has been identified by a deep RNA-sequencing approach in our previous study (Rola et al., 2006). In present study, we reported the altered circRNA expression profile in the traumatic cerebral cortex of mice following TBI. In fact, Xie et al. *(Xie et al., 2018)* and Jiang et al. *(Jiang et al., 2018)* recently has reported the altered expression of circular RNA in the traumatic cerebral cortex of mouse and rat after TBI. Xie et al. *(Xie et al., 2018)* applied a microarrays approach to figure out a total of 192 differentially expressed circRNAs (98 up-regulated and 94 down-regulated) in the traumatic cerebral cortex of SD rats at 3 h after TBI. We noted that Xie et al. *(Xie et al., 2018)* used fluid percussion brain injury to simulate TBI, which was different from our presently used CCI model. There was no overlap between the sequencing data of Xie et al. (Xie et al., 2018) and the present data, which may have resulted from the different genetic backgrounds, different TBI models and different end points. In addition, Jiang et al. (Jiang et al., 2018) recently applied the same deep RNA sequencing approach as the one employed in the present study to figure out a total of 191 differentially expressed circRNAs (98 up-regulated and 93 down-regulated) in the traumatic cerebral cortex of C57BL/6 mice at 6 h after TBI. In the study of Jiang et al. (Jiang et al., 2018), 1) TBI was induced by the CCI model; 2) the parameters were velocity 5.0 m/s; depth 2.0 mm and dwelling time 100 ms; 3) the end point to decapitate was 6 h post-TBI; and 4) the trauma was located in the left parietotemporal cortex. Compared to the study of Jiang et al. (Jiang et al., 2018), we used the same TBI model, the same CCI parameters and the same RNA-sequencing method in the same genetic background to detect the circRNA alteration post-TBI; however, our present end point was 24 h post-TBI, and the trauma was located in the right parietal lobe. Our present sequencing data were discrepant from that of Jiang et al. (Jiang et al., 2018), which may have resulted from the different end points, and different trauma locations. Moreover, Jiang et al. (Jiang et al., 2018) used a 5.5-mm diameter soft plastic film to cover the bone window, but we closed the bone window with bone wax. The plastic film was soft and could not completely close the cranial bone window, which could have relieved the elevated intra-cranial pressure (ICP) after TBI. The bone wax was tough and completely closed the bone window, resulting in a higher ICP. We inferred that the differential ICP post-TBI might also contribute to the discrepant circRNA expression. It is unfortunate that both Xie et al. *(Xie et al., 2018)* and Jiang et al. *(Jiang et al., 2018)* only performed the sequencing experiment with a subsequent biological analysis and did not further explore the function and possible mechanism of the circRNAs. In the present study, we preliminary found that the circRNA chr8_87,859,283–87,904,548 might play a role in secondary damage post-TBI *via* its potential pro-inflammatory effect, which might be not beneficial for neurological restoration after TBI. Nevertheless, all of these aforementioned studies (Xie et al., 2018; Jiang et al., 2018) jointly forecast that circRNAs may play important roles in the physiological and pathological processes post-TBI. Considering the reciprocal regulating relationship between circRNA, lncRNA and miRNA, future studies should nottarget the miRNA or lncRNA alone, as it would be wiser to combine circRNA with the other existing non-coding RNA to investigate the complex processes after TBI.

5. Conclusion

A total of 16 circRNAs were significantly changed in the traumatic cerebral cortex after TBI. Among them, the circRNA chr8_87,859,283–87,904,548 was significantly increased and potentially plays a pro-inflammatory role, which might cause a deleterious effect on neurological restoration after TBI.

Declaration of interest

The authors declare that no conflicts of interest exist.

Acknowledgements

This work was supported by grants from the National Natural Science Foundation of China (grant No.: 81571159) and the Youth Fund of the National Natural Science Foundation of China (grant No.: 81801230). We express special acknowledgement to “Chongqing Key Laboratory of Biochemistry and Molecular Pharmacology” for providing an experimental platform. We give special thanks to Rami Darwazeh from the First Affiliated Hospital of Chongqing Medical University for language modification.

Appendix A. Supplementary data

Supplementary data to this article can be found online at https://doi.org/10.1016/j.expneurol.2018.12.003.

References

Bai, Y., et al., 2018. Circular RNA DLGAP4 ameliorates ischemic stroke outcomes by targeting miR-143 to regulate endothelial-mesenchymal transition associated with blood-brain barrier integrity. J Neurosci 38 (1), 32–50. https://doi.org/10.1523/JNEUROSCI.1348-17.2017.

Bajrami, B., Zhu, H., Kwak, H.J., 2016 Sep 19a. G-CSF maintains controlled neutrophil mobilization during acute inflammation by negatively regulating CXCR2 signaling. J Exp Med. 213 (10), 1999–2018. https://doi.org/10.1084/jem.20160393.

Bajrami, B., et al., 2016b. G-CSF maintains controlled neutrophil mobilization during acute inflammation by negatively regulating CXCR2 signaling. J Exp Med 213 (10), 1999–2018. https://doi.org/10.1084/jem.20160393.

Bhat, S.A., et al., 2016. Angiotensin receptor blockade modulates NFkappaB and STAT3 Signaling and inhibits glial activation and neuroinflammation better than angiotensin-converting enzyme inhibition. Mol Neurobiol 53 (10), 6950–6967. https://doi.org/10.1007/s12035-015-9584-5.

Birney, E., et al., 2007. Identification and analysis of functional elements in 1% of the human genome by the ENCODE pilot project. Nature 447 (7146), 799–816. https://doi.org/10.1038/nature05874.

Cederberg, D., Siesjo, P., 2010. What has inflammation to do with traumatic brain injury? Childs Nerv Syst 26 (2), 221–226. https://doi.org/10.1007/s00381-009-1029-x.

Corps, K.N., Roth, T.L., McGavern, D.B., 2015. Inflammation and neuroprotection in traumatic brain injury. JAMA Neurol 72 (3), 355–362. https://doi.org/10.1001/jamaneurol.2014.3558.

Donofrio, G., et al., 2006. Outcome of bovine herpesvirus 4 infection following direct viral injection in the lateral ventricle of the mouse brain. Microbes Infect 8 (3), 898–904. https://doi.org/10.1016/j.micinf.2005.10.016.

Dubovicky, M., et al., 2014. Modulation of microglial function by the antidepressant drug venlafaxine. Interdiscip Toxicol 7 (4), 201–207. https://doi.org/10.2478/intox-2014-0029.

Guo, J., et al., 2016. Overexpression of fibulin-5 attenuates ischemia/reperfusion injury after middle cerebral artery occlusion in rats. Mol Neurobiol 53 (5), 3154–3167. https://doi.org/10.1007/s12035-015-9222-2.

Han, B., et al., 2018. Novel insight into circular RNA HECTD1 in astrocyte activation via autophagy by targeting MIR142-TIPARP: implications for cerebral ischemic stroke. Autophagy 14 (7), 1164–1184. https://doi.org/10.1080/15548627.2018.1458173.

Hansen, T.B., et al., 2013. Natural RNA circles function as efficient microRNA sponges. Nature 495 (7441), 384–388. https://doi.org/10.1038/nature11993.

Ho, J., et al., 2016. The involvement of regulatory non-coding RNAs in sepsis: a systematic review. Crit Care 20 (1), 383. https://doi.org/10.1186/s13054-016-1555-3.

Hsieh, C.Y., et al., 2014. Macrophage migration inhibitory factor triggers chemotaxis of CD74 + CXCR2+ NKT cells in chemically induced IFN-gamma-mediated skin inflammation. J Immunol 193 (7), 3693–3703. https://doi.org/10.4049/jimmunol.1400692.

Hu, J., et al., 2015. miR-126 promotes angiogenesis and attenuates inflammation after contusion spinal cord injury in rats. Brain Res 1608, 191–202. https://doi.org/10.1016/j.brainres.2015.02.036.

Huang, J.H., et al., 2016. Tetramethylpyrazine enhances functional recovery after contusion spinal cord injury by modulation of MicroRNA-21, FasL, PDCD4 and PTEN expression. Brain Res 1648 (Pt A), 35–45. https://doi.org/10.1016/j.brainres.2016.07.023.

Jiang, Y., et al., 2018. Circular RNA expression profile in mouse cortex after traumatic brain injury. J Neurotrauma 27 (10). https://doi.org/10.1089/neu.2018.5647.

Lei, P., et al., 2009. Microarray based analysis of microRNA expression in rat cerebral cortex after traumatic brain injury. Brain Res 1284, 191–201. https://doi.org/10.1016/j.brainres.2009.05.074.

Lerner, C.A., et al., 2016. Genetic ablation of CXCR2 protects against cigarette smoke-induced lung inflammation and injury. Front Pharmacol 7, 391. https://doi.org/10.3389/fphar.2016.00391.

Li, Z., et al., 2015. Exon-intron circular RNAs regulate transcription in the nucleus. Nat Struct Mol Biol 22 (3), 256–264. https://doi.org/10.1038/nsmb.2959.

Li, J., et al., 2018. High-throughput data of circular rna profiles in human temporal cortex tissue reveals novel insights into temporal lobe epilepsy. Cell Physiol Biochem 45 (2), 677–691. https://doi.org/10.1159/000487161.

Lin, S.P., et al., 2016. Circular RNA expression alterations are involved in OGD/R-induced neuron injury. Biochem Biophys Res Commun 471 (1), 52–56. https://doi.org/10.1016/j.bbrc.2016.01.183.

Liu, L., et al., 2014. Traumatic brain injury dysregulates microRNAs to modulate cell signaling in rat hippocampus. PLoS One 9 (8), e103948. https://doi.org/10.1371/journal.pone.0103948.

Loane, D.J., Faden, A.I., 2010. Neuroprotection for traumatic brain injury: translational challenges and emerging therapeutic strategies. Trends Pharmacol Sci 31 (12), 596–604. https://doi.org/10.1016/j.tips.2010.09.005.

Lukiw, W.J., 2013. Circular RNA (circRNA) in Alzheimer's disease (AD). Front Genet 4, 307. https://doi.org/10.3389/fgene.2013.00307.

Marchelletta, R.R., et al., 2015. Salmonella-induced diarrhea occurs in the absence of IL-8 Receptor (CXCR2)-dependent neutrophilic inflammation. J Infect Dis 212 (1), 128–136. https://doi.org/10.1093/infdis/jiu829.

Memczak, S., et al., 2013. Circular RNAs are a large class of animal RNAs with regulatory potency. Nature 495 (7441), 333–338. https://doi.org/10.1038/nature11928.

O'Connor, W.T., Smyth, A., Gilchrist, M.D., 2011. Animal models of traumatic brain injury: a critical evaluation. Pharmacol Ther 130 (2), 106–113. https://doi.org/10.1016/j.pharmthera.2011.01.001.

Qu, S., et al., 2015. Circular RNA: A new star of noncoding RNAs. Cancer Lett 365 (2), 141–148. https://doi.org/10.1016/j.canlet.2015.06.003.

Ranganathan, P., et al., 2013. CXCR2 knockout mice are protected against DSS-colitis-induced acute kidney injury and inflammation. Am J Physiol Renal Physiol 305 (10), F1422–F1427. https://doi.org/10.1152/ajprenal.00319.2013.

Rola, R., et al., 2006. Alterations in hippocampal neurogenesis following traumatic brain injury in mice. Exp Neurol 202 (1), 189–199. https://doi.org/10.1016/j.expneurol.2006.05.034.

Salvi, A., et al., 2016. Protective Effect of Tempol on Buthionine Sulfoximine-Induced Mitochondrial Impairment in Hippocampal Derived HT22 Cells. Oxid Med Cell Longev 2016, 5059043. https://doi.org/10.1155/2016/5059043.

Salzman, J., 2016. Circular RNA expression: its potential regulation and function. Trends Genet 32 (5), 309–316. https://doi.org/10.1016/j.tig.2016.03.002.

Sharma, A., et al., 2014. Identification of serum MicroRNA signatures for diagnosis of mild traumatic brain injury in a closed head injury model. PLoS One 9 (11), e112019. https://doi.org/10.1371/journal.pone.0112019.

Song, X., et al., 2016. Circular RNA profile in gliomas revealed by identification tool UROBORUS. Nucleic Acids Res 44 (9), e87. https://doi.org/10.1093/nar/gkw075.

Steele, C.W., et al., 2015. CXCR2 inhibition suppresses acute and chronic pancreatic inflammation. J Pathol 237 (1), 85–97. https://doi.org/10.1002/path.4555.

Szabo, L., et al., 2015. Statistically based splicing detection reveals neural enrichment and tissue-specific induction of circular RNA during human fetal development. Genome Biol 16, 126. https://doi.org/10.1186/s13059-015-0690-5.

Teng, Z., et al., 2016. Peroxisome proliferator-activated receptor beta/delta alleviates early brain injury after subarachnoid hemorrhage in rats. Stroke 47 (1), 196–205. https://doi.org/10.1161/STROKEAHA.115.011701.

Tiwari, N., et al., 2016. p53- and PAI-1-mediated induction of C-X-C chemokines and CXCR2: importance in pulmonary inflammation due to cigarette smoke exposure. Am J Physiol Lung Cell Mol Physiol 310 (6), L496–L506. https://doi.org/10.1152/ajplung.00290.2015.

Veno, M.T., et al., 2015. Spatio-temporal regulation of circular RNA expression during porcine embryonic brain development. Genome Biol 16, 245. https://doi.org/10.1186/s13059-015-0801-3.

Villapol, S., et al., 2012. Candesartan, an angiotensin II AT(1)-receptor blocker and PPAR-gamma agonist, reduces lesion volume and improves motor and memory function after traumatic brain injury in mice. Neuropsychopharmacology 37 (13), 2817–2829. https://doi.org/10.1038/npp.2012.152.

Werner, C., Engelhard, K., 2007. Pathophysiology of traumatic brain injury. Br J Anaesth 99 (1), 4–9. https://doi.org/10.1093/bja/aem131.

Wilhelm, B.T., et al., 2008. Dynamic repertoire of a eukaryotic transcriptome surveyed at single-nucleotide resolution. Nature 453 (7199), 1239–1243. https://doi.org/10.1038/nature07002.

Wu, F., et al., 2015a. CXCR2 is essential for cerebral endothelial activation and leukocyte recruitment during neuroinflammation. J Neuroinflammation 12, 98. https://doi.org/10.1186/s12974-015-0316-6.

Wu, F., et al., 2015b. CXCR2 is essential for cerebral endothelial activation and leukocyte recruitment during neuroinflammation. J Neuroinflammation 12 (98), 015–0316. https://doi.org/10.1186/s12974-015-0316-6.

Xia, S., et al., 2017 Nov 1. Comprehensive characterization of tissue-specific circular RNAs in the human and mouse genomes. Brief Bioinform. 18 (6), 984–992. https://doi.org/10.1093/bib/bbw081.

Xie, B.S., et al., 2018. Circular RNA expression profiles alter significantly after traumatic brain injury in rats. J Neurotrauma 35 (14), 1659–1666. https://doi.org/10.1089/neu.2017.5468.

You, X., et al., 2015. Neural circular RNAs are derived from synaptic genes and regulated by development and plasticity. Nat Neurosci 18 (4), 603–610. https://doi.org/10.1038/nn.3975.

Zhang, Y., et al., 2013. Circular intronic long noncoding RNAs. Mol Cell 51 (6), 792–806. https://doi.org/10.1016/j.molcel.2013.08.017.

Zhang, Q., et al., 2016. Aldose Reductase Regulates Microglia/Macrophages Polarization Through the cAMP Response Element-Binding Protein After Spinal Cord Injury in Mice. Mol Neurobiol 53 (1), 662–676. https://doi.org/10.1007/s12035-014-9035-8.

Zhang, X., Hamblin, M.H., Yin, K.J., 2018. Noncoding RNAs and stroke. Neuroscientist 1 (1073858418769556). https://doi.org/10.1177/1073858418769556.1073858418769556.

Zhong, J., et al., 2016. Altered expression of long non-coding RNA and mRNA in mouse cortex after traumatic brain injury. Brain Res 1646, 589–600. https://doi.org/10.1016/j.brainres.2016.07.002.

Zhong, J., et al., 2017a. Bexarotene protects against traumatic brain injury in mice partially through apolipoprotein E. Neuroscience 343, 434–448. https://doi.org/10.1016/j.neuroscience.2016.05.033.

Zhong, J., et al., 2017 Octb. The long non-coding RNA Neat1 is an important mediator of the therapeutic effect of bexarotene on traumatic brain injury in mice. Brain Behav Immun. 65, 183–194. https://doi.org/10.1016/j.bbi.2017.05.001.

Zhou, X., et al., 2016. MicroRNA-146a down-regulation correlates with neuroprotection and targets pro-apoptotic genes in cerebral ischemic injury in vitro. Brain Res 1648 (Pt A), 136–143. https://doi.org/10.1016/j.brainres.2016.07.034.

Zhu, L., et al., 2018. Circular RNA expression in the brain of a neonatal rat model of periventricular white matter damage. Cell Physiol Biochem 49 (6), 2264–2276. https://doi.org/10.1159/000493829.